*J. Earth Syst. Sci.* (2019)128:150
https://doi.org/10.1007/s12040-019-1187-5



# Palaeostress and magma pressure measurement of granite veins in the Neoproterozoic Ambaji granulite, South Delhi terrane, Aravalli–Delhi mobile belt, NW India: Implication towards the extension-driven exhumation of the middle–lower crustal rocks

Sudheer Kumar Tiwari* and Tapas Kumar Biswal

*Department of Earth Sciences, Indian Institute of Technology Bombay, Powai, Mumbai 400 076, India.*
**Corresponding author. e-mail: sudheer030192@gmail.com*

MS received 14 November 2018; revised 7 March 2019; accepted 20 March 2019

Neoproterozoic Ambaji granulite, in the South Delhi terrane (SDT) of the Aravalli–Delhi mobile belt (ADMB), is multiply deformed at different stages of its exhumation from the middle–lower crust. It was intruded by four phases of granites, $G_{0-3}$, of which the $G_3$ was syntectonic with brittle shearing. The orientation of the $G_3$ granite veins was used, in this paper, to measure the palaeostress and magma pressure during its intrusion. The $G_3$ granite has a porphyritic texture with quartz, microcline and biotite minerals and contains magmatic foliation; biotites are aligned oblique to such foliation, suggesting the syntectonic intrusion of the granite with normal faulting. Stereoplot of the poles of the granite veins shows concentration in the NW and SW quadrants and lack data over an elliptical area at the centre, indicating a girdle pattern. This implies that the magma pressure $P_m > \sigma_2$, compression $\sigma_1$ was vertical and extension $\sigma_3$ was NW–SE horizontal. Values of $\theta_2 = 16°$ and $\theta_3 = 40°$ were obtained from the stereoplot, used to calculate stress ratio $\Phi = 0.81$, driving pressure $R' = 0.92$ and the construction of the 3D Mohr plot for $P_m$ and principal stresses. Result suggests that the $G_3$ granite intruded under extensional tectonics that probably contributed to the exhumation of the Ambaji granulite.

**Keywords.** Palaeostress and magma pressure analysis; $G_3$ granite vein; extension; exhumation; Neoproterozoic Ambaji granulite; Aravalli–Delhi mobile belt.

## 1. Introduction

Stress and strain are two fundamental parameters of deformation in the lithosphere. Stress indicates the dynamic part where an external force acts on a rock mass creating deformation. Strain is the kinematic part that includes the change in the shape, size or volume in ductile deformation or rock failure in brittle deformation (Ramsay 1967; Twiss and Moores 2007; Fossen 2010). There are several methods available in the literature to measure the strain (Ramsay and Huber 1987), but it is challenging to measure the absolute value of stress. The measurement of stress provides information regarding compression, extension and strike slip tectonic settings and helps in understanding the tectonic history of a terrane, like basin formation, inversion of basin, exhumation of deeper rocks, intrusion of dyke and vein, etc. In the literature, several methods have been proposed to measure the stress ratio

Published online: 04 June 2019

$\Phi = (\sigma_2 - \sigma_3)/(\sigma_1 - \sigma_3)$ (Angelier 1994; Ramsay and Lisle 2000; Fossen 2010), magmatic pressure $P_m$ relative to the tectonic stress and the driving stress ratio $R' = (P_m - \sigma_3)/(\sigma_1 - \sigma_3)$. This is done in several ways: (i) using grain size and shape in ductile deformation (Stipp *et al.* 2002; Stipp and Tullis 2003); (ii) fault-slip data in brittle deformation (Anderson 1951) and (iii) distribution pattern of dykes and veins (Baer *et al.* 1994; Jolly and Sanderson 1997).

In this paper, palaeostress and magmatic pressure of granite veins have been measured to understand the tectonics of granite intrusion. Our study area belongs to the Neoproterozoic Ambaji granulite which is one of such exhumed blocks within the vast stretch of low-grade rocks of the South Delhi terrane (SDT) of the Aravalli–Delhi mobile belt (ADMB), NW India. Previous studies on the Ambaji granulite include folding, metamorphism, geochemistry, strain analysis of shear zones and palaeostress analysis of faults. In this study, we focus on $G_3$ granite veins which have intruded during brittle shearing. The orientation of the $G_3$ veins has been used to deduce the palaeostress and magmatic pressure during its intrusion, using techniques developed by Baer *et al.* (1994) and Jolly and Sanderson (1997). The tectonics of granite intrusion has been correlated with the tectonics of the exhumation of the granulite.

## 2. Tectonic setting of the Ambaji granulite

### 2.1 *Regional geology*

The NE–SW trending ADMB contains several geologically distinct terranes demarcated by shear zones (figure 1a and b; Gupta *et al.* 1980; Singh *et al.* 2010). The terranes are, namely, Archaean Hindoli–Jahajpur, Mangalwar, Sandmata terranes, the Palaeo-Mesoproterozoic Aravalli and North Delhi terranes, and the Neoproterozoic Sirohi and SDT. The Hindoli–Jahajpur terrane consists of greenstone belts, the Mangalwar terrane has a tonalite–trondhjemite–granodiorite (TTG) gneiss and the Sandmata terrane includes granulite facies rocks (Gupta *et al.* 1980; Sinha-Roy 1985; Bhowmik *et al.* 2010). The Aravalli and North Delhi terranes comprise quartzite–pelite–carbonate rocks metamorphosed in greenschist to lower amphibolite facies. Ophiolite-bearing Rakhabdev shear zone in Aravalli and Andean-type continental arc magmatism in North Delhi provides evidence of subduction during the Palaeo-Mesoproterozoic period (Deb and Thorpe 2001; Kaur *et al.* 2009). The SDT comprises extensive quartzite–pelite–carbonate metasediments with oceanic rocks such as rift-related metabasalt and metarhyolite, diorite and plagiogranite (ca. 1000 Ma; Volpe and Macdougall 1990; Dharma Rao *et al.* 2013). These rocks, by and large, are metamorphosed under greenschist to amphibolite facies. There is a unique occurrence of granulitic rocks near Ambaji (Ambaji granulite) that has been studied in this paper. The sedimentation age in SDT was between ca. 1200 and 860 Ma and the age of metamorphism was ca. 860 Ma (Biswal *et al.* 1998a, b; Singh *et al.* 2010). The Sirohi terrane comprises isolated outcrops of low-grade metasedimentary rocks of ca. 900 and 820 Ma age (Purohit *et al.* 2012; Dharma Rao *et al.* 2013). The Sirohi terrane has undergone multiple phases of deformation and granitic intrusion between ca. 860 and 750 Ma (e.g., Erinpura granite, ca. 860–730 Ma, Crawford (1975); Choudhary *et al.* (1984); Balda granite, ca. 770 Ma, Sarkar *et al.* (1992); Tosham granite, ca. 820 Ma, Murao *et al.* (2000); and Malani igneous suite, ca. 770 Ma, Gregory *et al.* (2009) and de Wall *et al.* (2012, 2014)). The Malani igneous suite is the most prominent among them, which has intruded along extensional fractures (Sharma 2005). Furthermore, Sindreth and Punagarh basins hosting volcano-sedimentary sequences (ca. 765 Ma) were deposited in the extensional setting (figure 1b; Bhardwaj and Biswal 2018).

### 2.2 *Geology of the Ambaji granulite*

#### 2.2.1 *Rock types*

The Ambaji granulite includes pelitic, calcareous and mafic granulite (figure 2; Biswal *et al.* 1998a, b; Sarkar 2006; Singh *et al.* 2010) with narrow stripes of schist and amphibolite along shear zones. The pelitic granulite is a migmatitic rock (figure 3a); the melanosome contains spinel, cordierite, sillimanite, garnet and biotite and the leucosome contains quartz, plagioclase and K-feldspar. The calcareous granulite shows a rib structure due to differential weathering and contains diopside, scapolite, calcite, plagioclase and wollastonite. The mafic granulite consists of orthopyroxene, clinopyroxene, plagioclase and hornblende; garnet is absent in the assemblage. Relict pods of gabbro and norite, interpreted as the protolith of the mafic granulite occurs in the area (Biswal *et al.* 1998a).

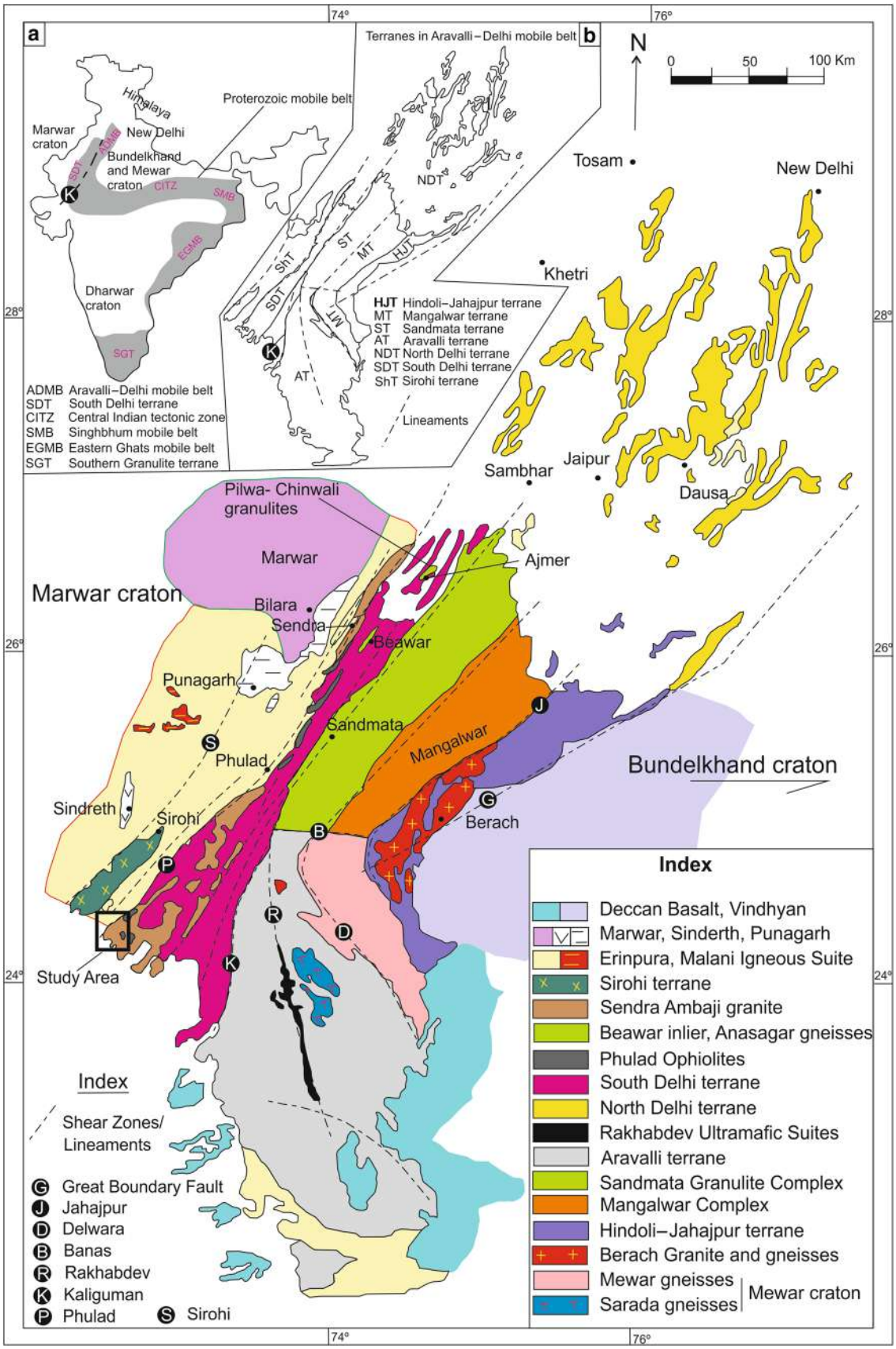


Figure 1. Geological map of the ADMB with different terranes and shear zones: (**a**) location of Proterozoic mobile belts in India, including the ADMB and (**b**) simplified map of the ADMB showing different terranes. K – Kaliguman shear zone defines the subduction zone of the SDT (modified after Singh *et al.* 2010).

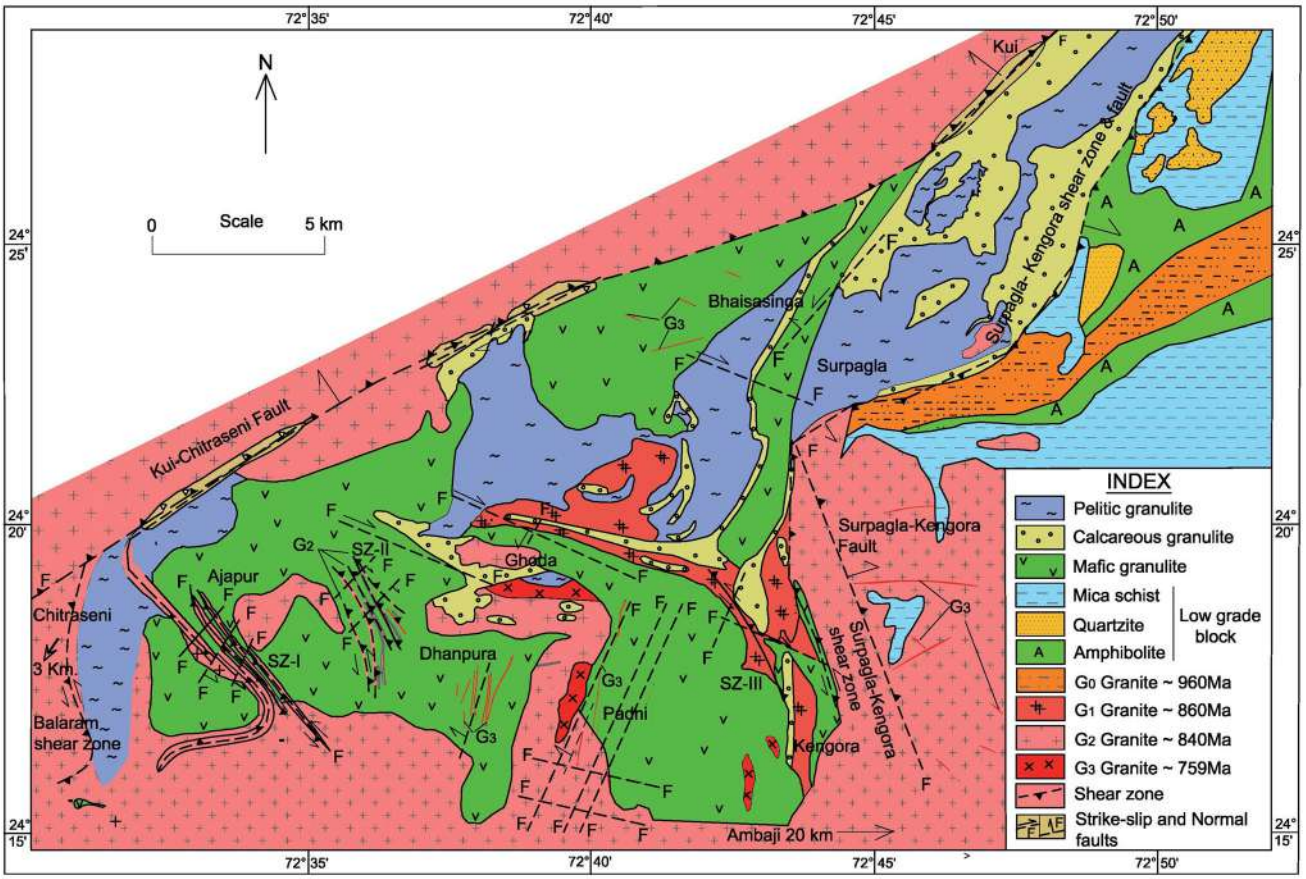


Figure 2. Geological map of the Ambaji granulite (modified after Singh *et al.* 2010).

### 2.2.2 *Folding-metamorphism*

Granulite has undergone three phases of folding (Singh *et al.* 2010). The first phase of folding is represented by isoclinal and recumbent $F_1$ folds with the NE–SW axis, which was developed on the bedding ($S_0$) by a sub-horizontal simple shear. $F_1$ is associated with penetrative axial planar gneissosity, $S_1$, which is defined by the parallel arrangement of granulite grade minerals as sillimanite, spinel, cordierite and garnet in pelitic granulite; diopside, plagioclase and wollastonite in calcareous granulite, and orthopyroxene, clinopyroxene and hornblende in mafic granulite. Migmatitic banding was developed parallel to the $S_1$ fabric (figure 3a). These features suggest that the granulite facies metamorphism and melting of the metasediments were syn-$F_1$. The mineral assemblage in the pelitic granulite indicates a PT of $\geq 850$°C and 5.5–6.8 kbar for peak granulite facies metamorphism that occurred at the middle–lower crust at nearly 25-km depth (Singh *et al.* 2010). The $F_1$ folds were coaxially refolded by the NE–SW striking open upright $F_2$ folds producing a type 3 interference pattern. $F_2$ folds were produced by the NW–SE compression. Spaced crenulation cleavage, microlithons and a set of shear bands axial planar to the $F_2$ fold developed during the $F_2$ folding, defining the $S_2$ fabric (figure 3a). A number of large-scale syn-$F_2$ shear zones (figure 2), namely, the Balaram shear zone, Surpagla–Kengora shear zone and SZ-I, SZ-II and SZ-III running for tens of kilometres with thicknesses varying from tens of metres to hundreds of metres, were developed. Shear zones were retrogressive, and hosted greenschist grade mylonite. The mylonite contains subhorizontal stretching lineations defined by stretched quartz and biotite grains. On the XZ section of the mylonite cut parallel to the stretching lineation and perpendicular to mylonitic foliation, the K-feldspar porphyroclasts indicate top-to-the-NW sinistral shearing (figure 3b). Furthermore, multiple phases of pseudotachylites were generated by the frictional melting along the shear zone (figure 3c). Some of them were deformed into ultramylonites. The parallel association of deformed and undeformed pseudotachylites indicates a transitional deformation from brittle to

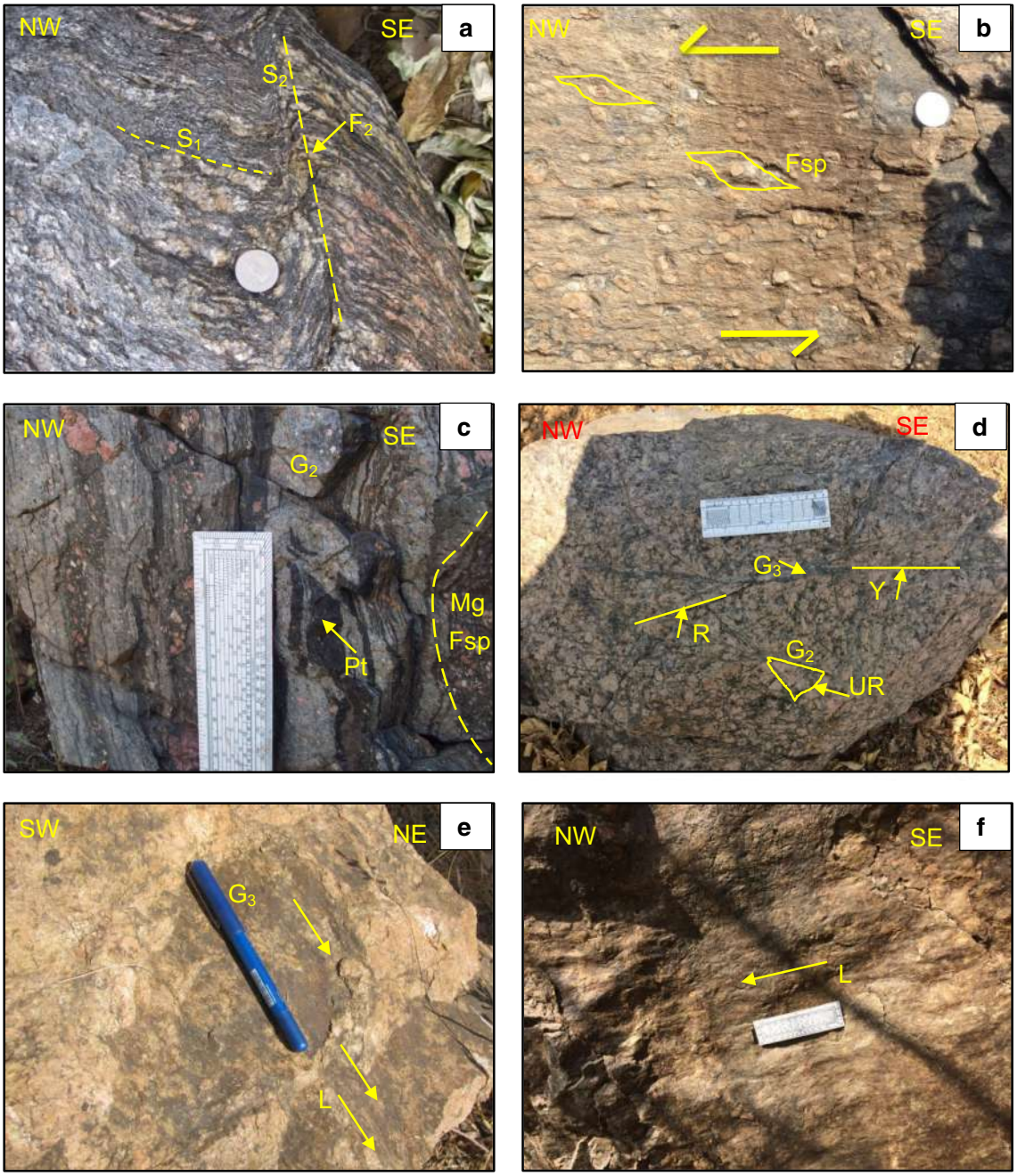


Figure 3. Field photographs: (**a**) Pelitic granulite with migmatitic structures, $S_1$ fabric is indicated by migmatitic layers, the $S_1$ fabric is folded and sheared parallel to the $F_2$ fold, vertical section; (**b**) $S_2$ sinistral-top-to-NW shear in the Surpagla–Kengora shear zone, indicated by sigma type feldspar porphyroclasts (Fsp), horizontal section; (**c**) pseudotachylite veins (Pt) within $G_2$ granite mylonite, mafic granulite (Mg) is in contact with $G_2$. Pt is deformed as indicated by deformed clasts within it, feldspathisation (Fsp) is present within mafic granulite, vertical section; (**d**) fracture within $G_2$ granite, Y shear indicates main shear while R indicates Riedel shear, thin $G_3$ vein has intruded, minor saussuritisation in the $G_2$ granite is seen in contact with the $G_3$ vein, UR – undeformed rock within a network of fractures, horizontal section; (**e**) near vertical slickenlines defined by dark pulverised material in the $G_3$ granite, indicating a normal slip, (L), arrows indicate slip direction, vertical section and (**f**) horizontal slickenlines, marked by arrow, indicate strike slip, vertical section.

ductile and back to brittle regime, suggesting the exposure of a palaeo–brittle–ductile transition zone (e.g. Price *et al.* 2012). Hence the granulite was exhumed from the middle–lower crust to the BDT zone during the $F_2$ folding. Exhumation produced a decompression texture in the granulite; smaller cordierite and spinel grains developed around the $F_1$ garnet porphyroblasts, and kyanite

and andalusite were developed from $F_1$-sillimanite. Subsequently, NW–SE striking upright large wavelength $F_3$ folds developed due to the NE–SW compression that brought a large-scale variation in the strike of the litho units and shear zones, and a reversal of the plunging of the $F_1$ and $F_2$ folds producing Type 1 and Type 2 interference patterns. Granulites are marked by several sets of faults and fractures, the Kui–Chitraseni fault and Surpagla–Kengora faults border the granulite block.

#### 2.2.3 *Granite and geochronology*

Several phases of granite ($G_{0–3}$) have intruded the granulite. Approximately 960 Ma $G_0$ granite intruded during sedimentation and was folded and metamorphosed (Singh *et al.* 2010). Approximately 860 Ma $G_1$ granite intruded during the $F_1$ folding and is gneissic in character. It occurs as interlayered bands within metasediments and shows a medium to coarse-grained texture consisting of quartz, feldspar, biotite, garnet and sillimanite. It was produced from the melting of the pelitic granulite (figure 3a). Approximately 840 Ma $G_2$ granite occurs as veins as well as batholiths showing equigranular and rapakivi texture with quartz, feldspar and biotite minerals (figures 3c and 4b, d). The $G_2$ intrusion is synkinematic with the $F_2$ folding; it has metasomatised the adjacent country rock and K-feldspar crystals are crystallised (Fsp) along the foliation plane of the mafic granulite (figure 3c). $G_2$ is mylonitised along shear zones. Approximately 759 Ma old $G_3$ granite occurs as veins (figure 4a and b) which is the focus of this study. They have intruded along the faults, fractures and foliations. We have used the orientation of the fractures and granite veins to estimate the palaeostress and magmatic pressure at the time of intrusion of the $G_3$ granite.

## 3. Methodology

### 3.1 *Palaeostress analysis*

Dykes and veins intrude when the magmatic pressure exceeds the tectonic stress across the weak plane such as the fracture plane. This can be denoted as $P_m \geq \sigma_n$, where $P_m$ stands for magmatic pressure and $\sigma_n$ stands for normal stress acting on the weak plane (Baer *et al.* 1994; Jolly and Sanderson 1997). The fractures perpendicular to $\sigma_3$ were more dilated since $\sigma_3$ is the least tectonic stress. The planes at right angles to the $\sigma_2$ and $\sigma_1$ are the least dilated. When $P_m$ exceeds the value of $\sigma_1$, all fractures are dilated, and veins intrude in several orientations. If $P_m \geq \sigma_2$, veins occur in all other orientations but for horizontal or gentle dipping veins. In that situation in a stereoplot, veins are plotted near the periphery and remain absent over the elliptical area in the centre (Jolly and Sanderson 1997; Mondal and Mamtani 2013; Martinez-Poza *et al.* 2014). This is known as the girdle distribution pattern. The centre of the void area indicates $\sigma_1$. The minimum angle between the dilated fracture and the $\sigma_1$ and $\sigma_2$ direction ($\theta_2$, $\theta_3$, respectively) can be measured from the stereoplot. If $P_m < \sigma_2 > \sigma_3$, poles of the veins show clustering around $\sigma_3$ axis. In that situation, the minimum angle between the dilated fracture and $\sigma_2$ and $\sigma_3$ direction ($\theta_1$, $\theta_2$, respectively) can be measured. Depending upon the relative value of $P_m$ with tectonic stress, different stereoplots are obtained. Stereoplot provides $\theta_1$, $\theta_2$ and $\theta_3$ values which are used to construct the 3D Mohr plot to display the $P_m$ values with respect to $\sigma_1, \sigma_2$ and $\sigma_3$. Furthermore, the stress ratio '$\Phi$' for different situations can be computed from the following equations (Jolly and Sanderson 1997; Mondal and Mamtani 2013; Martinez-Poza *et al.* 2014):

For $P_m < \sigma_2$,

$$\Phi = (\sigma_2 - \sigma_3)/(\sigma_1 - \sigma_3) = (1 + \cos 2\theta_2)/(1 + \cos 2\theta_3). \quad (1)$$

For $P_m > \sigma_2$,

$$\Phi = (\sigma_2 - \sigma_3)/(\sigma_1 - \sigma_3) = 1 - \{(1 - \cos 2\theta_2)/(1 - \cos 2\theta_3)\}. \quad (2)$$

The driving pressure ratio $R'$ that describes the magnitude of the magmatic pressure relative to the tectonic stress is given by the formula (Jolly and Sanderson 1997)

$$R' = (P_m - \sigma_3)/(\sigma_1 - \sigma_3) = (1 + \cos 2\theta_2)/2. \quad (3)$$

The above principle has been applied by several researchers to perform palaeostress analysis (e.g., André *et al.* 2001; McKeagney *et al.* 2004; Mazzarini and Isola 2007; Mazzarini *et al.* 2011; Mondal and Mamtani 2013; Martinez-Poza *et al.* 2014; Lahiri and Mamtani 2016). We measured the attitude of fractures and granite veins in the field and plotted poles, in a stereonet. Post-$G_3$ fractures,

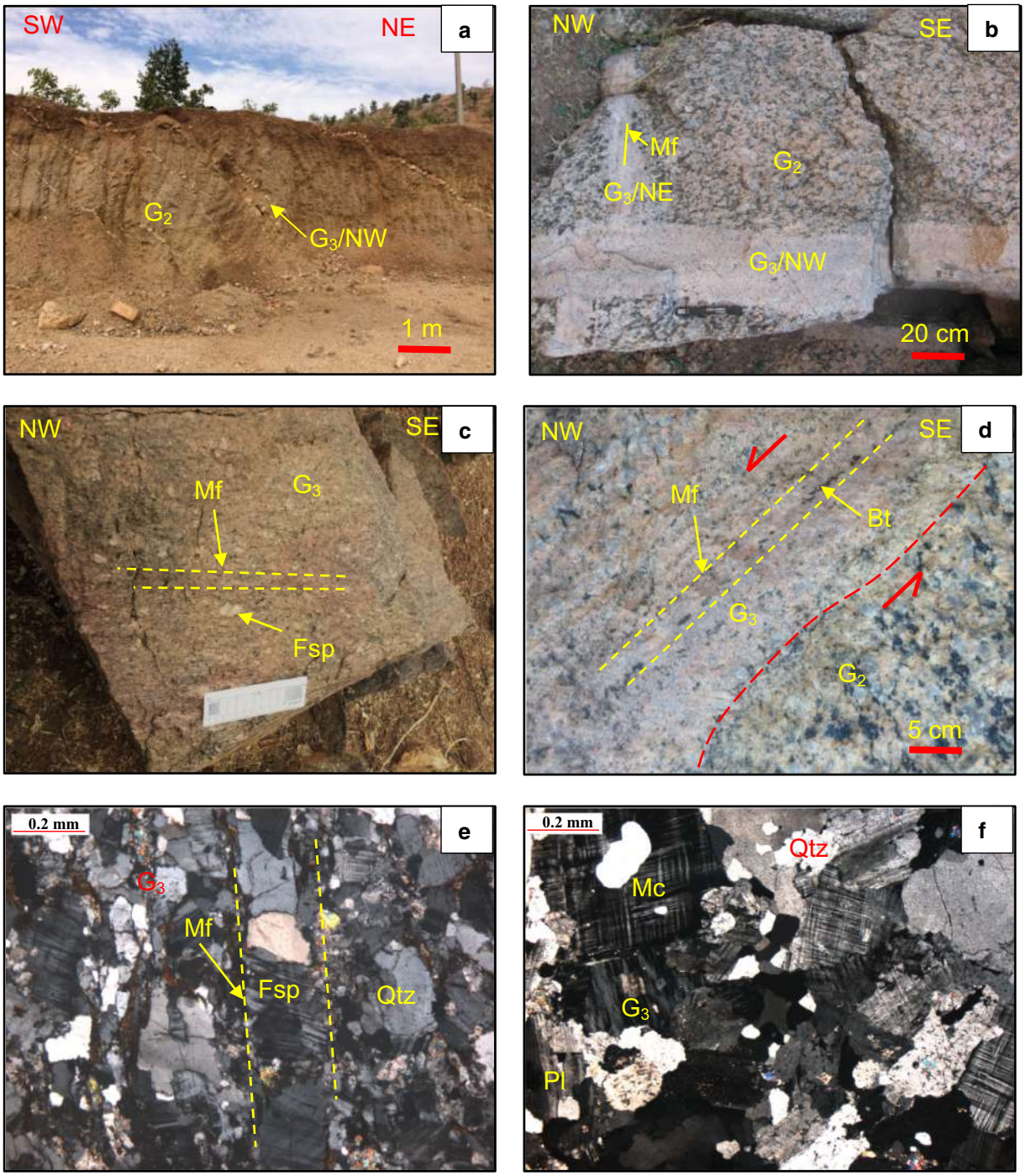


Figure 4. (**a**) Field photographs of NE – moderately inclined $G_3$ granite veins cross-cutting the $G_2$ granite near Kengora, vertical section; (**b**) two sets of $G_3$ veins (NE, NW striking) cross-cutting the $G_2$ granite, one set shows magmatic foliation (Mf), horizontal section, (**c**) $G_3$ granite veins showing magmatic foliation (Mf) defined by parallel arrangement of quartz, feldspar (Fsp) and biotite in layers, (**d**) NW–$G_3$ granite vein in the $G_2$ granite, contact is marked by a red-dashed line, $G_3$ contains magmatic foliation (Mf), biotite grains (Bt) in the magmatic layer are obliquely arranged to magmatic foliation (Mf), suggesting a normal slip, marked by a red arrow, vertical section; (**e**) a photomicrograph showing magmatic foliation (Mf) due to the alignment of quartz (Qtz), feldspar (Fsp) and biotite grains, undulose extinction is seen in quartz due to high temperature deformation during the intrusion of the $G_3$ granite syntectonic to normal slip, but there is no dynamic recrystallisation and (**f**) the hypidiomorphic texture in the core of the $G_3$ granite (Mc: microcline, Pl: plagioclase and Qtz: quartz).

which cross-cut the granite veins, were excluded from the analysis as far as possible.

## 4. Results

### 4.1 *Faults and fractures*

We used the geological map prepared by Singh *et al.* (2010) for plotting the faults, fractures and granite veins (figure 2). Two major normal faults, namely, the NE–SW to the NNW–SSE Surpagla–Kengora fault and the NE–SW Kui–Chitraseni faults are located in the east and west margin of the granulite block (figure 2). They are inclined away from the granulite block giving rise to a horst structure to the block. In addition to these boundary faults, several internal faults in the WNW–ESE and NE–SW directions occur in the area. The width of the faults and fractures vary from a few millimetres to metres. Fault outcrops are characterised by blocky rocks traversed by several fractures (figure 3d; Riedels, Y shears). They host cataclasites containing angular clasts set within a glassy to an ultra-comminuted matrix. Thin films of dark pulverised material form slickenlines on the fracture surface, in addition to the ridges in groove lineations (figure 3e and f). Mineral growth is rarely seen along the fracture. Between the sets of fractures, islands of undeformed rock occur (figure 3d). It is therefore interpreted that the faulting has taken place within a purely brittle zone. Two types of slickenlines are observed. Vertical slickenlines correspond to a normal slip (figure 3e); there are also horizontal slickenlines indicating a strike slip (figure 3f). In several occasions, the overprinting of the vertical lineation on the horizontal lineation has been preserved, suggesting the normal slip was post-kinematic to the strike slip. Stereoplot of poles to 1162 faults and fractures shows random distribution (figure 5a) and the Rose diagram reveals the NE–SW prominent orientation and the NW–SE is subordinate (figure 5c). A preliminary study suggests that the NW–SE extension was probably responsible for brittle faulting. The faults and fractures are intruded by $G_3$ granite veins (figure 3d), showing saussuritisation at places (figure 3d).

### 4.2 $G_3$ *granite veins*

Multiple phases of $G_3$ granite veins have intruded the granulites and $G_{0–2}$ granites along pre-existing fractures (figure 4a and b). These are abundant around Dhanpura, Padni, Kengora and Bhaisasinga areas (figure 2). We have analysed the granite veins of Dhanpura, Padni and Kengora areas for their close proximity. Stereoplot and Rose diagram of 698 veins suggest that the NE–SW and NW–SE sets are more prominent (figure 5b and d). The veins mutually cross-cut each other suggesting their broad synchronous character (figure 4b). Veins are steep to moderately inclined; horizontal/subhorizontal veins are absent. The veins have tabular geometry; the width of the veins varies from a few centimetres to tens of metres and the strike-length varies from a few metres to a kilometre. In many instances, the veins contain magmatic foliation/layering parallel to the vein wall, produced from the shapes of preferred orientation of quartz, plagioclase, microcline and biotite phenocrysts (figure 4c and d). The biotite grains are concentrated in layers where the individual grains have been obliquely arranged to magmatic foliation consistent with the normal slip (figure 4d). Furthermore, plagioclase and quartz from the vein margin display undulose extinction suggesting solid-state deformation; however, there is no dynamic recrystallisation (figure 4e). The core of the veins preserves the hypidiomorphic and porphyritic texture (figure 4f). Furthermore, fractures are developed close to the vein margin parallel to magmatic foliation, and the vein walls have been marked by normal slip slickenlines (figure 4e). Based on these features, we interpret that the intrusion of the $G_3$ granite is syntectonic with normal faulting.

### 4.3 *Palaeostress*

Stereoplot for fracture planes produced distribution all over the net (figure 5a) while $G_3$ granite veins showed a girdle pattern with an elliptical void area at the centre (figure 5b). Girdle pattern suggests the magnitude of magmatic pressure $P_m > \sigma_2$. Following Jolly and Sanderson (1997), the centre of the ellipse represents $\sigma_1$ direction, the $\sigma_3$ lies at the highest cluster in the NW part of the plot and $\sigma_2$ lies on the great circle passing through the longer dimension of the ellipse.

From figure 5(b), $\theta_2 = 16°$ and $\theta_3 = 40°$ were obtained; these are the angles between the pole of the dilated fracture planes with $\sigma_1$ on the $\sigma_3$–$\sigma_1$ and $\sigma_2$–$\sigma_1$ planes, respectively.

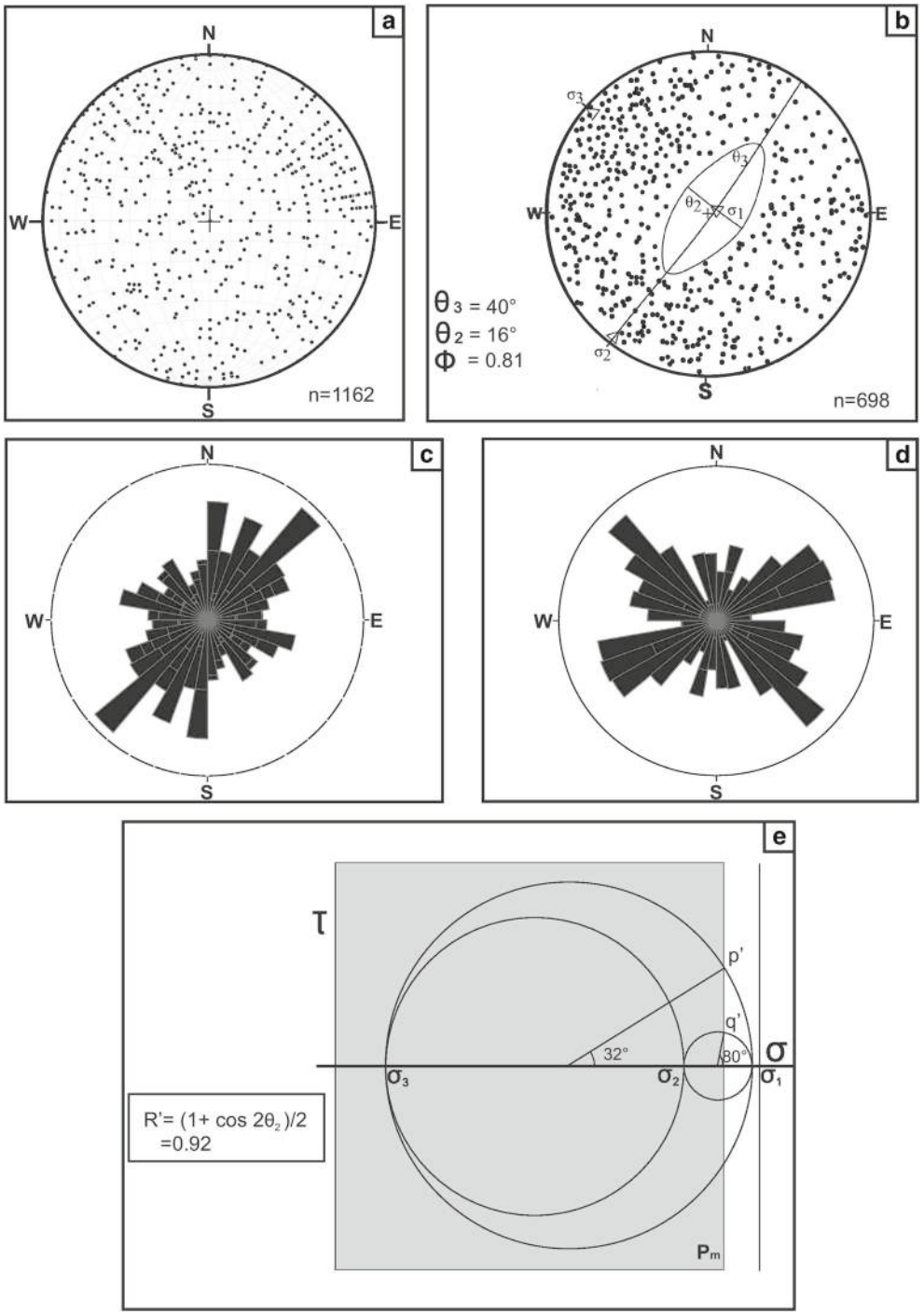


Figure 5. Palaeostress determination from the $G_3$ granite veins: (**a**) stereoplot of poles of fractures (1162 data) in the granulite and the $G_{0–2}$ granites show orientation in all directions, some are even horizontal; (**b**) stereoplot of poles of the $G_3$ granite veins (698 data) shows prominent NE–SW and NW–SE directions, with a subordinate amount in other directions, horizontal veins are absent indicated by the elliptical void area at the centre, and this is known as girdle distribution, which means the horizontal fractures are not dilated, and the centre of the ellipse represents $\sigma_1$ direction, $\sigma_3$ lies in the NW–SE quadrants, $\sigma_2$ in the NE–SW quadrants, $\theta_2 = 16°, \theta_3 = 40°$ are measured from ellipse axes and $\Phi = 0.81$ is calculated from equation (1); (**c**) Rose diagram for fractures and faults (1162), the NE–SW direction is more prominent than the NW–SE direction, (**d**) Rose diagram for the $G_3$ granite veins (698), NE–SW and NW–SE directions are prominent and (**e**) 3D Mohr plot for the $G_3$ granite veins, $\theta$ values are obtained from figure b. $R' = 0.92$ is calculated from equation (3). The $P_m$ field is shaded. $P_m$ value exceeds that of $\sigma_2$ but is less than $\sigma_1$. (On the procedure to draw the figure, refer to the text.)

For $P_m > \sigma_2$,

$$\Phi = (\sigma_2 - \sigma_3)/(\sigma_1 - \sigma_3)$$
$$= 1 - \{(1 - \cos 2\theta_2)/(1 - \cos 2\theta_3)\} = 0.81,$$
$$R' = (P_m - \sigma_3)/(\sigma_1 - \sigma_3) = (1 + \cos 2\theta_2)/2 = 0.92.$$

Hence $R' > \Phi$. This indicates that the $G_3$ granite was emplaced in an axial tension setting implying vertical compression and horizontal extension in all directions. However, from the data concentration in figure 5(b), the NW–SE was the dominant extension direction. The $\theta_2$ and $\theta_3$ angles were used to construct a 3D Mohr plot. An arbitrary circle was drawn between $\sigma_3$ and $\sigma_1$ (figure 5e) and $2\theta_2 = 32^\circ$ had been plotted in the above circle, and point $p'$ was obtained. Fractures making a higher angle were dilated. The $P_m$ value was obtained from the projection of $p'$ on the horizontal axis; accordingly, the $P_m$ field was shaded. Another circle was drawn between $\sigma_2$ and $\sigma_1$ in such a manner that when the $2\theta_3 = 80^\circ$ angle was plotted, the point $q'$ would lie on the same alignment as $p'$, so that fractures making a higher angle would be dilated. The figure indicates $P_m > \sigma_2 < \sigma_1$.

## 5. Discussion

### 5.1 *Stress pattern*

The Ambaji granulite represents the middle–lower crustal rocks in the entire 800 km stretch of the low-to-medium grade SDT. The maximum extension during the $G_3$ intrusion lay in the NW–SE direction. The majority of the granite veins intruded in NE–SW direction as the fractures in that direction were most dilated. The next major set of veins were in the NW–SE direction right angle to $\sigma_2$ direction. As the $P_m$ exceeded $\sigma_2$ value, fractures in that direction were also dilated. Gentle dipping fractures (<16°) did not dilate as they were making a high angle with $\sigma_1$ which was $> P_m$. Girdle pattern ($R' > \Phi$) indicates $P_m > \sigma_2 < \sigma_1$. The stress ratio $\Phi = 0.81$ and the driving stress ratio was 0.92 suggesting axial tension. Hence, the granulitic crust was undergoing an axial tension, dominantly in the NW–SE direction, during the intrusion of the $G_3$ granite.

### 5.2 *Tectonic implications*

Ambaji granulite was metamorphosed under granulite facies at ca. 860 Ma in a compressive setting during the South Delhi orogeny (Biswal *et al.* 1998a, b; Singh *et al.* 2010). NW–SE shortening during the $F_1$ and $F_2$ folding, plutonism due to $G_2$ intrusion and transpression during $S_2$ shearing thickened the crust and built the great height of the orogen. Thickening of the crust accompanied by denudation brought the first stage of exhumation/uplift to a 15-km depth. This is evident in the mineral assemblages of the decompressed granulite and the brittle–ductile $S_2$ shear zones. Subsequently, granulite underwent extensional tectonics and developed faults and fractures. $G_3$ granite was intruded along these faults and fractures. Palaeostress analysis suggests axial extension (dominantly the NW–SE extension) during the $G_3$ intrusion.

Several mechanisms have been explained for the exhumation of deeper rocks, e.g., granite intrusion and vertical thrusting (e.g., Hill *et al.* 1995; Ring *et al.* 1999), transpressive shearing in a zone of oblique convergence (e.g., Sylvester and Smith 1976; Sanderson and Marchini 1984; Fossen and Tikoff 1993; Martelat *et al.* 1997; Thompson *et al.* 1997) and crustal extension causing stretching and tectonic denudation (e.g., Dewey 1988; Dewey *et al.* 1998). Exhumation of the Ambaji granulite consists of two stages, in the first, it was exhumed by thrusting to the BDT zone. Second, in the brittle crust, the exhumation took place by extension. Palaeostress and magma pressure measurement of the $G_3$ granite confirms such extensional setting during brittle deformation. In addition, strike slip faults and normal faults develop in the extensional setting. Hence, it is interpreted that exhumation through the brittle crust was due to the NW–SE extension. The orogenic trend of the ADMB is NE–SW which was produced from the NW–SE compression. The extension during brittle deformation was NW–SE that was nearly at a right angle to the orogenic trend. Probably, at the end of compressional tectonics, the orogen went through stress relaxation in the same direction as the compression-producing extension.

Extensional tectonics in the Ambaji granulite has been studied for the first time. More work on extensional tectonics is yet to be done in the ADMB. Several basement rocks are exposed in Beawar and further north, which need investigation in light of extensional tectonics. Multiple phases of granite within SDT may be due to extension-induced decompression melting. A preliminary study mentions that the adjoining

Sirohi terrane had experienced a Neoproterozoic extension (Sharma 2005) that created the N–S fractures and ca. 750 Ma Malani igneous suite intruded along such fractures. Sindreth and Punagarh volcano-sedimentary basins were created in the extensional fault-bounded grabens (figure 1b; Bhardwaj and Biswal 2018). Decompression melting induced by such extension probably gave rise to the Malani igneous suite (Eby and Kochhar 1990; Maheshwari *et al.* 2001; Wang *et al.* 2017). The $G_3$ granite could be due to the decompression melting induced by extension (e.g., Auzanneau *et al.* 2006).

As far as global correlation is concerned, ADMB is shown to be connected to other parts of the Gondwanaland Supercontinent (Singh *et al.* 2010). For instance, the East African orogen, Seychelles, Madagascar and the Arabian–Nubian shield were in continuity with the ADMB. These continents had experienced ca. 750 Ma old magmatism (Tucker *et al.* 1999; Torsvik *et al.* 2001; Ashwal *et al.* 2002; Jöns *et al.* 2006; Biswal *et al.* 2007; Thomas *et al.* 2009; Singh *et al.* 2010 and references therein). Hence, it is likely that Neoproterozoic extensional tectonics was common to all these continents.

## 6. Conclusions

The Ambaji granulite represents an exhumed middle–lower crustal metamorphic complex within the low–medium grade SDT. The exhumation/uplift of the granulite was a two-stage process: in the first stage, it was exhumed to the BDT zone by thrusting. In the second stage, it was exhumed to the surface by extension. The second stage of exhumation was due to the extension which is well represented by normal faults and $G_3$ granite veins. From the palaeostress analysis of the ca. 759 Ma $G_3$ granite veins, a NW–SE extension was interpreted which matches with that of the brittle faults in the area. This suggests that the ADMB crust was stretched in the NW–SE direction right angle to the orogen-length that probably led to the exhumation of the granulite to the surface. Extensional tectonics was probably operative during this period in other continents, namely, the East African orogen, Seychelles, Madagascar and the Arabian–Nubian shield in Gondwanaland, which were in continuity with the ADMB during the Neoproterozoic period.

## Acknowledgements

The first author acknowledges the research funding through the UGC-SRF fellowship from New Delhi. The authors sincerely thank the Department of Science and Technology, New Delhi and the Indian Institute of Technology Bombay for funding the project. Prof Jeremie Lehmann, Prof Helga de Wall, Prof R Harinarayan and Prof Frederico Meira Faleiros critically reviewed the earlier version of the paper and significantly contributed to its improvement. We are extremely grateful to them. We acknowledge the help of Neeraj Sharma during the fieldwork. A critical review by Prof Manish Mamtani, IIT Kharagpur and an anonymous reviewer and editorial handling by Prof Rajneesh Bhutani are gratefully acknowledged.

## References

Anderson E M 1951 *The dynamics of faulting*; Oliver and Boyd, Edinburgh Vol. **195**, no. **1**, 206p.

André A S, Sausse J and Lespinasse M 2001 New approach for the quantification of paleostress magnitudes: Application to the Soultz vein system (Rhine graben, France); *Tectonophys.* **336** 215–231.

Angelier J 1994 Fault slip analysis and palaeostress reconstruction; In: *Continental deformation* (ed.) Hancock P L, Pergamon Press, Oxford, pp. 53–101.

Ashwal L D, Demaiffe D and Torsvik T H 2002 Petrogenesis of Neoproterozoic granitoids and related rocks from the Seychelles: The case for an Andean-type arc origin; *J. Petrol.* **43** 45–83.

Auzanneau E, Vielzeuf D and Schmidt W 2006 Experimental evidence of decompression melting during exhumation of subducted continental crust; *Contrib. Mineral. Petrol.* **152** 125–148.

Baer G, Beyth M and Reches Z E 1994 Dikes emplaced into fractured basement, Timna igneous complex, Israel; *J. Geophys. Res.: Solid Earth* **99** 24,039–24,050.

Bhardwaj A and Biswal T K 2018 Deformation and tectonic history of Punagarh basin in the Trans-Aravalli Terrane of North-Western India; In: *Geological evolution of the Precambrian Indian Shield*, Springer, Cham., pp. 159–178.

Bhowmik S K, Bernhardt H J and Dasgupta S 2010 Grenvillian age high-pressure upper amphibolite–granulite metamorphism in the Aravalli–Delhi mobile belt, northwestern India: New evidence from monazite chemical age and its implication; *Precamb. Res.* **178** 168–184.

Biswal T K, Gyani K C, Parthasarathy R and Pant D R 1998a Implications of the geochemistry of the Pelitic Granulites of the Delhi Supergroup, Aravalli Mountain Belt, Northwestern India; *Precamb. Res.* **87** 75–85.

Biswal T K, Gyani K C, Parthasarathy R and Pant D R 1998b Tectonic implication of geochemistry of gabbro-norite-basic granulite suite in the Proterozoic Delhi Supergroup, Rajasthan, India; *J. Geol. Soc. India* **52** 721–732.

Biswal T K, De Waele B and Ahuja H 2007 Timing, dynamics of the juxtaposition of the Eastern Ghats Mobile Belt against the Bhandara Craton, India: A structural, zircon U–Pb SHRIMP study of the fold–thrust belt, associated nepheline syenite; *Tectonics* **26** TC4006, https://doi.org/10.1029/2006TC002005.

Choudhary A K, Gopalan K and Sastry C A 1984 Present status of the geochronology of the Precambrian rocks of Rajasthan; *Tectonophys.* **105** 131–140.

Crawford A R 1975 Rb–Sr age determination for the Mount Abu Granite, related rocks of Gujarat; *J. Geol. Soc. India* **16** 20–28.

Deb M and Thorpe R I 2001 Geochronological constraints in the Precambrian geology of Northwestern India and their metallogenic implication; In: *Pre-seminar volume on international workshop on sediment-hosted lead-zinc sulfide deposit in the northwestern Indian shield, Delhi-Udaipur, India* (eds) Deb M and Goodfellow W D, Prepared at Dept. of Geology, Delhi University, New Delhi, pp. 137–152.

de Wall H, Pandit M K, Dotzler R and Just J 2012 Cryogenian transpression, granite intrusion along the western margin of Rodinia (Mt. Abu region): Magnetic fabric, geochemical inferences on Neoproterozoic geodynamics of the NW Indian block; *Tectonophys.* **554** 143–158.

de Wall H, Pandit M K, Sharma K K, Schöbel S and Just J 2014 Deformation, granite intrusion in the Sirohi area, SW Rajasthan – Constraints on cryogenian to Pan-African crustal dynamics of NW India; *Precamb. Res.* **254** 1–18.

Dewey J F 1988 Extensional collapse, orogen; *Tectonics* **7** 1123–1139.

Dewey J F, Holdsworth R E and Strachan R A 1998 Transpression and transtension zones; *Geol. Soc. London, Spec. Publ.* **135** 1–14.

Dharma Rao C V, Santosh M, Kim S W and Li S 2013 Arc magmatism in the Delhi fold belt, SHRIMP U–Pb zircon ages of granitoids, implications for Neoproterozoic convergent margin tectonics in NW India; *J. Asian Earth Sci.* **78** 83–99.

Eby G N and Kochhar N 1990 Geochemistry, petrogenesis of the Malani igneous suite, North Peninsular India; *J. Geol. Soc. India* **36** 109–130.

Fossen H 2010 *Structural geology*; Cambridge University Press, Cambridge, 463p.

Fossen H and Tikoff B 1993 The deformation matrix for simultaneous simple shearing, pure shearing and volume change, and its application to transpression–transtension tectonics; *J. Struct. Geol.* **15** 413–422.

Gregory L C, Meert J G, Bingen B, Pandit M K and Torsvik T H 2009 Paleomagnetism, geochronology of the Malani Igneous Suite, Northwest India. Implications for the configuration of Rodinia, the assembly of Gondwana; *Precamb. Res.* **170** 13–26.

Gupta S N, Arora Y K, Mathur R K, Iqbalduddin, Prasad B, Sahai T N and Sharma S B 1980 Lithostratigraphic map of the Aravalli region, Hyderabad, India; *Geol. Surv. Ind. Hyderabad.*

Hill K C, Hill K A, Cooper G T, O'Sullivan A J, O'Sullivan P B and Richardson M J 1995 Inversion around the Bass basin, SE Australia; *Geol. Soc. London, Spec. Publ.* **88** 525–547.

Jolly R J H and Sanderson D J 1997 A Mohr circle construction for the opening of a pre-existing fracture; *J. Struct. Geol.* **19** 887–892.

Jöns N, Schenk V, Appel P and Razakamanana T 2006 Two-stage metamorphic evolution of the Bemarivo Belt of northern Madagascar: Constraints from reaction textures and *in situ* monazite dating; *J. Met. Geol.* **24** 329–347.

Kaur P, Chaudhari N, Raczek I, Kröner A and Hofmann A W 2009 Record of 1.82 Ga, Andean-type continental arc magmatism in NE Rajasthan, India: Insights from zircon, Sm–Nd ages, combined with Nd–Sr isotope geochemistry; *Gondwana Res.* **16** 56–71.

Lahiri S and Mamtani M A 2016 Scaling the 3-D Mohr circle and quantification of paleostress during fluid pressure fluctuation – Application to understand gold mineralization in quartz veins of Gadag (southern India); *J. Struct. Geol.* **88** 63–72.

Maheshwari A, Sia1 A N, Coltorti M, Chittora V K, Manoel J M and Cruz M J M 2001 Geochemistry and Petrogenesis of Siwana Peralkaline Granites, West of Barmer, Rajasthan, India; *Gondwana Res.* **4** 87–95.

Martelat J E, Nicollet C, Lardeaux J M, Vidal G and Rakotondrazafy R 1997 Lithospheric tectonic structures developed under high-grade metamorphism in the southern part of Madagascar; *Geodinamica Acta* **10** 94–114.

Martinez-Poza A I, Druguet E, Castaño L M and Carreras J 2014 Dyke intrusion into a pre-existing joint network: The Aiguablava lamprophyre dyke swarm (Catalan coastal ranges); *Tectonophys.* **630** 75–90.

Mazzarini F and Isola I 2007 Hydraulic connection and fluid overpressure in upper crustal rocks: Evidence from the geometry and spatial distribution of veins at Botrona quarry, southern Tuscany, Italy; *J. Struct. Geol.* **29** 1386–1399.

Mazzarini F, Musumeci G and Cruden A R 2011 Vein development during folding in the upper brittle crust: The case of tourmaline-rich veins of eastern Elba Island, northern Tyrrhenian Sea, Italy; *J. Struct. Geol.* **33** 1509–1522.

McKeagney C J, Boulter C A, Jolly R J H and Foster R P 2004 3-D Mohr circle analysis of vein opening, Indarama lode-gold deposit, Zimbabwe: Implications for exploration; *J. Struct. Geol.* **26** 1275–1291.

Mondal T K and Mamtani M A 2013 3-D Mohr circle construction using vein orientation data from Gadag (southern India) – Implications to recognize fluid pressure fluctuation; *J. Struct. Geol.* **56** 45–56.

Murao S, Deb M, Takagi T, Seki Y, Pringle M and Naito K 2000 *Geochemical, geochronological constraints for tin polymetallic mineralization in Tosham area, Haryana, India; crustal evolution, metallogeny in the northwestern Indian shield*; Narosa Publishing House, New Delhi, pp. 430–442.

Price N A, Johnson S E, Gerbi C C and West D P 2012 Identifying deformed pseudotachylyte and its influence on the strength and evolution of a crustal shear zone at the base of the seismogenic zone; *Tectonophys.* **518** 63–83.

Purohit R, Papineau D, Kröner A, Sharma K K and Roy A B 2012 Carbon isotope geochemistry, geochronological constraints of the Neoproterozoic Sirohi Group from northwest India; *Precamb. Res.* **220** 80–90.

Ramsay J G 1967 *Folding and fracturing of rocks*; McGraw-Hill Book Company, New York, 568p.

Ramsay J G and Huber M I 1987 *The techniques of modern structural geology*; Vol. **2**, Academic Press, London.

Ramsay J G and Lisle R J 2000 *Applications of continuum mechanics in structural geology, techniques of modern structural geology*; Vol. **3**, Academic Press, London.

Ring U, Brandon M T, Willett S D and Lister G S 1999 Exhumation processes; In: *Exhumation processes: Normal faulting, ductile flow, erosion* (eds) Ring U, Brandon M T, Lister G S and Willett S D, *Geol. Soc. London, Spec. Publ.* **154** 1–27.

Sanderson D J and Marchini W R D 1984 Transpression; *J. Struct. Geol.* **6** 449–458.

Sarkar S 2006 Deformational history of Delhi supergroup of rocks around Siyawa, Sirohi district, Rajasthan, NW India; PhD Thesis.

Sarkar S C, Gupta A and Basu A 1992 North Singhbhum Proterozoic Mobile Belt, Eastern India: Its character, evolution, metallogeny; In: *Metallogeny related to tectonics of the Proterozoic Mobile Belts* (ed.) Sarkar S C, Oxford, IBH, New Delhi, pp. 271–305.

Sharma K K 2005 Malani magmatism: An extensional lithospheric tectonic origin; *Geol. Soc. Am.* **388** 463–476.

Singh Y K, De Waele B, Karmarkar S, Sarkar S and Biswal T K 2010 Tectonic setting of the Balaream–Kui–Surpagla–Kengora granulites of the Aravalli Mobile Belt, NW India, its implication on correlation with the East African Orogen in the Gondwana assembly; *Precamb. Res.* **183** 669–688.

Sinha-Roy S 1985 Granite-greenstone sequence, geotectonic development of SE Rajasthan; *Bull. Geol. Min. Metal. Soc. India* **53** 115–123.

Stipp M and Tullis J 2003 The recrystallized grain size piezometer for quartz; *Geophys. Res. Lett.* **30** 2088.

Stipp M, Stünitz H, Heilbronner R and Schmid S M 2002 The eastern Tonale fault zone: A 'natural laboratory' for crystal plastic deformation of quartz over a temperature range from 250 to 700°C; *J. Struct. Geol.* **24** 1861–1884.

Sylvester A G and Smith R R 1976 Tectonic transpression and basement-controlled deformation in San Andreas fault zone, Salton Trough, California; *Am. Assoc. Pet. Geol. Bull.* **60** 2081–2102.

Thomas R J, De Waele B, Schofield D I, Goodenough K M, Horstwood M, Tucker R, Bauer W, Annells R, Howard K, Walsh G and Rabarimanana M 2009 Geological evolution of the Neoproterozoic Bemarivo Belt, northern Madagascar; *Precamb. Res.* **172** 279–300.

Thompson A B, Schulmann K and Jezek J 1997 Thermal evolution and exhumation in obliquely convergent (transpressive) orogens; *Tectonophys.* **280** 171–184.

Torsvik T H, Ashwal L D, Tucker R D and Eide E A 2001 Neoproterozoic geochronology and palaeogeography of the Seychelles microcontinent: The India link; *Precamb. Res.* **110** 47–59.

Tucker R D, Ashwal L D, Handke M J, Hamilton M A, Le Grange M and Rambeloson R A 1999 U–Pb geochronology and isotope geochemistry of the Archean and Proterozoic rocks of north-central Madagascar; *J. Geol.* **107** 135–153.

Twiss R J and Moores E M 2007 *Structural geology*; © WH Freeman and Company, New York, 532p.

Volpe A M and Macdougall J D 1990 Geochemistry, isotopic characteristics of mafic (Phulad ophiolite), related rocks in the Delhi supergroup, Rajasthan, India: Implications for rifting in the Proterozoic; *Precamb. Res.* **48** 167–191.

Wang W, Cawood P A, Zhou M F, Pandit M K, Xia X P and Zhao J H 2017 Low-$\delta^{18}$O Rhyolites from the Malani igneous suite: A positive test for south China, NW India linkage in Rodinia; *Geophys. Res. Lett.* **44**(**20**) 10,298–10,305.

Corresponding editor: Rajneesh Bhutani